BEXUS 23 OSCAR: Solar Cell I-V Monitoring System for Space Environments

Peer-reviewed author version

NAGELS, Steven; CARDINALETTI, Ilaria; CORNELISSEN, Rob; SCHREURS, Dieter; VANGERVEN, Tim; VODNIK, Jelle; HRUBY, Jaroslav; NESLADEK, Milos; MANCA, Jean & DEFERME, Wim (2017) BEXUS 23 OSCAR: Solar Cell I-V Monitoring System for Space Environments. In: Proceedings of the 23rd ESA Symposium on European Rocket and Balloon programmes and related research,p. 1-6.

BEXUS 23 OSCAR: SOLAR CELL I-V MONITORING SYSTEM FOR SPACE ENVIRONMENTS

S. Nagels [1] [2], I. Cardinaletti [1] [3], R. Cornelissen [4], D. Scheurs [1] [3], T. Vangerven [1] [3], J. Vodnik [1] [3], J. Hruby [1] [3], M. Nesladek [1] [3], J. V. Manca [4], and W. Deferme [1] [2]

[1] Hasselt University, Istitute for Materials Reseach (IMO), Wetenschapspark 1, 3590 Diepenbeek, Belgium
wim.deferme@uhasselt.be
[2] Flanders Make vzw, Oude Diestersebaan 133, 3920 Lommel, Belgium
wim.deferme@uhasselt.be
[3] IMEC vzw – Division IMOMEC, Wetenschapspark 1, 3590 Diepenbeek, Belgium
wim.deferme@uhasselt.be
[4] Hasselt University, XLAB, Agoralaan gebouw D, 3590 Diepenbeek, Belgium
jean.manca@uhasselt.be

ABSTRACT

Novel thin film solar cells exhibit unprecedented specific power, which is a key figure of merit for space applications. To get a first indication of their possible degradation in space environments, the OSCAR ('Optical Sensors based on CARbon materials') team has built a solar cell performance monitoring system and deployed it on the BEXUS 23 flight. This paper reports the design, testing and performance of said system. Our system performed impeccably over its 4h mission course, maintaining communication and reliably reporting solar cell I-V curves. It forms a guideline for anyone who needs to measure millivolts and microamperes in similar conditions, monitor solar cells on remote locations or wants to follow up on degradation of thin film solar cells in space.

1. INTRODUCTION

1.1. Background

Solar energy is consistently used for powering long-term spacecraft missions ever since the launch of the Vanguard 1C satellite in 1958 [1]. Alternatives such as batteries and RTG's are undesirable either due to short depletion time or public health risks on reentry. Specific power – watts per kg – remains the main selection parameter since launch costs are mainly calculated on a per kilogram basis. Thick, rigid gallium-arsenide cells pose the current de facto standard because they are known for their reliability and high power per square meter. However, based on specific power, they are trumped by new generations of thin film solar cells (i.e. polymer, small molecule, perovskite). Usage of these novel cells in aerospace applications is still non-existent due to their unknown reliability. This is exactly the property OSCAR ('Optical Sensors based on CARbon materials') monitored during the BEXUS23 flight.

1.2. Monitoring reliability of solar cells

Each solar cell is characterized by its I-V curve. This curve typically resembles a dark current elbow shape which shifts down under the influence of light-generated current – also known as 'photocurrent' – and shows the currents and corresponding voltages at which the solar cell operates [2]. Along this curve, a specific point can be found for which the output power is highest. This point on the I-V curve is called the maximum power point (MPP). Together with the open circuit voltage V_{oc} and the short circuit current I_{sc}, the MPP can be used to calculate the solar cell's power conversion efficiency. By observing changes in I_{sc}, V_{oc} and MPP over time, we can monitor how the solar cells behave over the course of our flight.

Six different kinds of solar cells were selected for the experiment, each with its own range of currents and voltages as depicted in Tab. 1. Current ranges are taken from dark current beyond the 1 sun V_{oc} up to 50% over the photocurrent reached at 1 sun.

Table 1 – Solar cell samples included in our experiment along with their operating voltage and current ranges.

#	Cell Type	Voltage [V]		Current [mA]	
		min	max	min	max
A	IPV	0.00	7.00	-119	411
B	$MAPbI_3$	0.00	1.00	-6.75	3.50
C	$PBDTTPD:PC_{71}BM$	0.00	1.00	-3.00	14.0
D	$PCPDTQx(2F):PC_{71}BM$	0.00	0.85	-3.00	3.50
E	$F4\text{-}ZnPc:C_{60}$	0.00	0.85	-1.07	2.80
F	$DCV5T:C_{60}$	0.00	1.00	-1.05	2.10

The monitoring system should be able to take measurements within these ranges at optimal measuring resolution. 20 equidistant voltages should be applied from the devices' voltage range while measuring the corresponding current.

1.3. Implications of space environment

Since the experiment had to go into space, both mechanical dimensions and weight became a constraint. The flight we designed for had a cruising altitude of 25km and floating time of 2h. Temperatures would reach as low as -70ºC, pressures 10mbar and the gondola would be rotating. Furthermore, we would have a 100W EBASS and a 10W E-Link transmitter emitting lots of interference at respectively 30m and less than 1m from our measuring setups. All these factors had to be taken into account when designing our measuring setup.

2. DESIGN

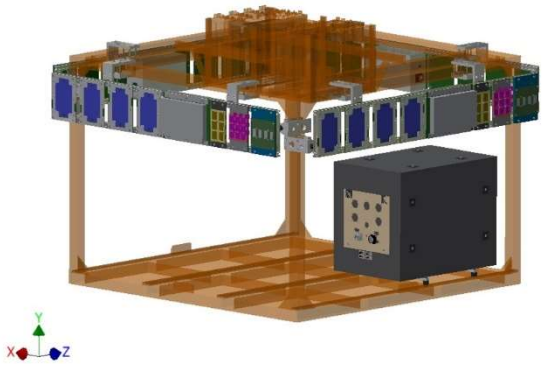

Figure 1 – Mechanical design of the OSCAR project on the BX23 gondola. Each side is equipped with an I-V measuring panel. Sample positions indicated in blue (type A), yellow (types B-C-D) and pink (types E-F).

2.1. System level design choices

We decided to place identical but independent measuring units on all 4 sides of the gondola. By doing this, we make sure at least one panel is in direct sunlight at any given time. Each of these panels contains 64 devices: 8 UHasselt PBDTTPD:$PC_{71}BM$, 8 UHasselt PCPDTQx(2F):$PC_{71}BM$, 8 IMEC $MAPbI_3$, 24 IAPP F4-ZnPc:C_{60}, 12 IAPP DCV5T:C_{60} and 4 Infinity PV cells. Measuring a point from the I-V curve requires first the application of a voltage step from the cell's operating range (through DAC) and secondly analog read of this applied voltage as well as its corresponding solar cell current (through 2 separate ADC's). A single circuit capable of measuring a solar cell I-V curve thus consists of at least 1 DAC for applying voltage and 2 ADC's respectively for measuring voltage and current.

2.2. Measuring board level design choices

To perform measurements with the highest possible precision, we had to match the solar cell I-V ranges to the selected Arduino Due microcontroller board's analog in- and outputs. It provided 2 12bit DAC (0.55 to 2.75V output) and 12 12bit ADC (0 to 3.3V input) channels. If we combine the number of chosen samples, their I-V ranges and the number of ADC channels at hand, three sample groups can be made. Each sample group corresponds to a (number of) measuring circuit(s) with fixed gain and offset values to match the broad, bipolar range of the solar cell signals to the limited, unipolar range of signals with which the microcontroller can work. Tab. 2 shows all three sample groups along with their current and voltage ranges.

2.3. Single measuring circuit design

Since channels were limited, we chose our measuring strategy to use a single DAC channel which supplies 20 equidistant voltages from its output range to all subcircuits. From there on, 6 differential amplifier circuits offset and rescale this voltage according to Eq. 1:

$$V_O = (R_2 / R_1) * (V_2 - V_1) \quad (1)$$

In this way the applied voltage then corresponds to the requested voltage range for each of the sample groups it is applied to. Within each sample group circuit, both this applied voltage as well as the corresponding solar cell current are then measured through each their own ADC channel. For the solar cell current signal, a transimpedance amplifier first performs a conversion from current to voltage following Eq. 2.

$$V_O = -R * I_{in} \quad (2)$$

Then a matching is performed again by shifting and rescaling differential amplifier circuits according to Eq. 1, be it this time of the current and voltage signals from the solar cell to the input of the microcontroller's ADC. Each measuring circuit supports up to 16 devices through an analogue multiplexing stage.

Table 2 – Sample groups with their corresponding measuring ranges and theoretical resolutions, respectively for voltage and current.

#	Voltage [V]		V LSB [mV]	Current [mA]		I LSB [µA]
	min	max		min	max	
A	0.00	7.00	1.709	-300	500	170.9
BCF	0.00	1.00	0.244	-6.00	14.0	4.883
DEdiode	0.00	0.85	0.208	-5.00	5.00	2.441

Compromises were made in current measuring resolution where needed in order to group certain solar cell types together. Since we scale the current and voltage ranges to the complete input voltage of the 12bit ADC's, we can calculate the theoretical measuring resolutions. These are depicted along with the voltage and current measuring ranges in Tab. 2.

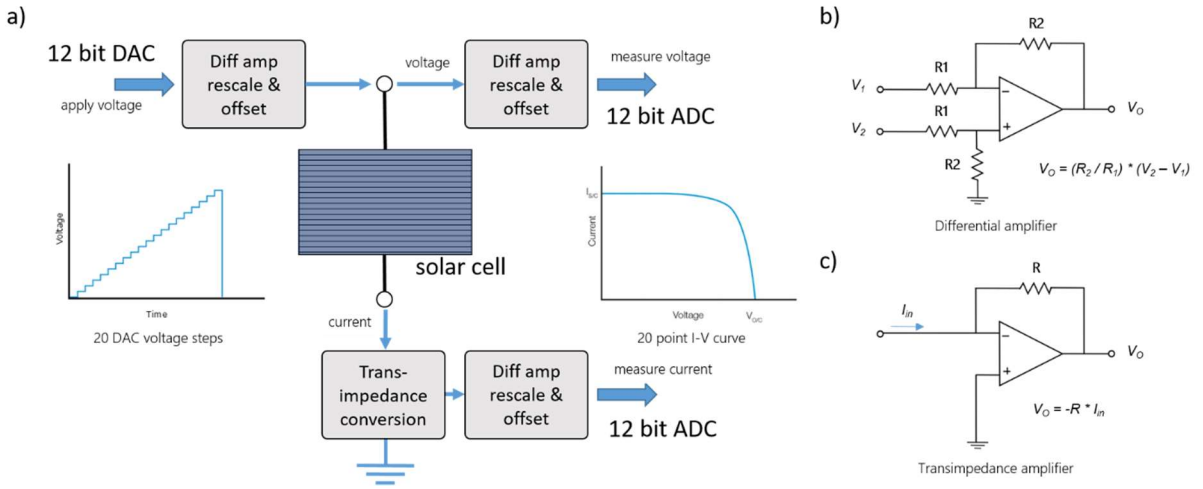

Figure 2 – a) High level circuit description of a single sample group measuring circuit (multiplexing stage not shown for the sake of clarity) b) Basic differential amplifier rescale & offset circuit c) Basic transimpedance amplifier circuit.

As can be derived from Tab. 2, solar cell sample groups were named according to the letter designations of the cell types from Tab. 1. Furthermore a reference silicon photodiode was included in the DE sample group, hence 'DEdiode'.

2.4. Software flow panels

A simple state machine is used for the control software running on the measurement boards. This enables us to recover to a certain state from intermittent power interruptions.

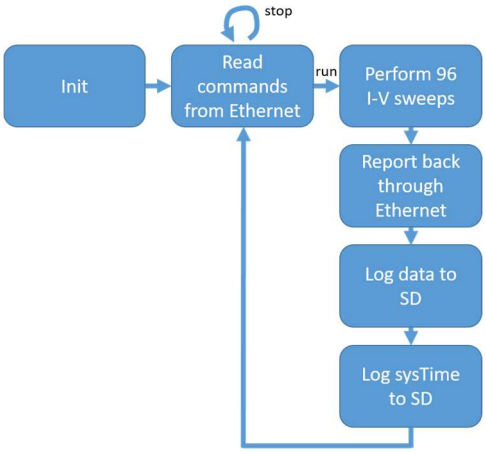

Figure 3 – Measuring panel software flow chart

Upon powering up, the system checks in its non-volatile memory (SD card) which was the last recorded previous state and total runtime and recovers it to SRAM. In a first loop step, pending commands from ground station (GS) are handled. When the system is on halt, this will be the only loop step. From the moment on a 'run' command is received, the system goes into active state, records this state change in flash, and subsequently measures a 20 point I-V curve for each of the 96 channels, sends these measurement values down to ground station, creates a local back-up of the data in flash and logs current system runtime to flash.

2.5. Ground station software

The GS consists of a LabVIEW program which is able to send commands to the measuring panels, receive and log their sent down data and display the last reported I-V sweeps for each panel.

3. IMPLEMENTATION

Figure 4 – Fully populated measuring panel with measurement board's metallic enclosure removed.

3.1. Electromechanical co-design

A single I-V panel consists out of one measuring board accompanied by 7 sample contacting PCB's: 4 on the left and 3 on the right as shown in Fig. 4. Connecting traces run from the measuring board through PCI-e edge connectors across the contacting boards to spring loaded contacts. The samples are placed on top of these spring loaded contacts and held in place by Teflon brackets. This whole stack, PCB–sample–bracket, is then screw fastened with bolts and T-nuts to a frame of strut profiles. By implementing in this way, we employ our circuit boards both for carrying the electrical connections as well as the mechanical load of the samples and their brackets. By relying solely on PCB's and edge connectors, we create very robust connections throughout the entire system and a minimum build and

(dis)assembly time. Not a single wire connection was used to implement the measuring panels.

3.2. Shielding considerations

A typical BEXUS experiment is inherently bound to radio frequent transmission: be it of housekeeping data, experiment communications, air traffic transponder or post cut down GPS tracker. All these RF transmitters are promising culprits of electromagnetic interference (EMI) noise in our measuring setup. Tab. 3 lists all different sources with characteristics most important to our setup.

Table 3 – Inherent sources of EMI on board the BEXUS 23 flight. ATC stands for Air Traffic Transponder.

EMI source	TX freq. [MHz]	Power [W]	Distance [m]
E-Link	2400 – 2500	10	< 1
E-BASS	402.2	100	30
ATC	1090	200	30
GPS tracker	1615	0.1	< 1

Aside from these inherently present EMI sources, only a single experiment on board transmits RF signals. This is the diamond based magnetometer which forms the second part of the OSCAR experiment. It transmits microwaves in the range of 2700 to 3000 MHz at 0.063W and less than 1m from the measuring panels.

All in all we can conclude that some form of EMI shielding is adequate considering the amount of EMI sources, their power and proximity. For this reason, all connecting boards have fully copper poured ground planes on the top and bottom layers which are stitched together with vias every 10mm ($\lambda/10$ for f = 3GHz) around the edges of the board. It effectively creates a Faraday cage around the traces which connect measurement board to samples and thus reduces the surface susceptible to EMI to the contact points and samples themselves. The measuring board is completely enclosed in a metallic enclosure which acts as a shield. The PCB copper pour shielding layers, strut profile frame and measuring board enclosure are all connected through to the ground terminal of the measuring board's isolating DC/DC converter. Each frame is furthermore mounted with electrically isolating rubber bumpers to the gondola.

3.3. Measuring board overview

Our measuring board has an Arduino Due at heart and is surrounded by 6 measuring circuits, each supporting 16 devices through analog multiplexers. ADG1406 multiplexers were used because of their +-15V rail to rail operation, 300mA continuous current support, 3V logic compatible inputs and 9.5Ω on resistance. Sample group A however exceeds the current supported by ADG1406 and is therefore outfitted with G3VM-61 MOSFET relays with 500mA continuous current support and 1Ω on resistance on each multiplexing channel. The relays are driven one at a time by the 16 multiplexer channels and, when selected, connect to the measuring circuit.

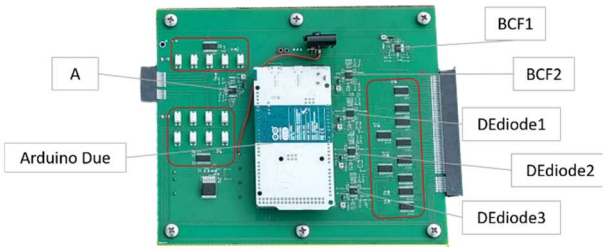

Figure 5 – Indication of measuring board subcircuits and microcontroller board. Multiplexing stages in red outlined shapes. Notice the white MOSFET relays included at sample group A's measuring circuit.

4. FLIGHT

The BEXUS23 gondola ultimately launched on the 7th of October 2016 at 07:07:26 UTC. It reached its cruising altitude of 32km after about 2h flight time and remained at this altitude for just over 2.5h. Air pressure dropped steadily with altitude and reached a minimum of 6hPa. Temperatures dropped to a minimum of -56.8°C in the tropopause.

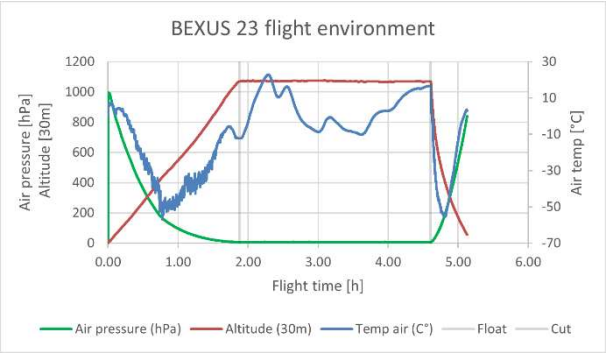

Figure 6 – BX23 flight data. Air pressure shown in green, altitude in red and air temperature in blue. Float phase starts at 1h52m. Cut-down performed at 4h36m into the flight. Courtesy of the Swedish Space Corporation (SSC).

The system performed steadily over the entire course of the flight until at 4h15m flight time I-V measurements shown at ground station appeared corrupted and shortly after communications were also lost. Post flight failure analysis however proved this was caused by battery drainage. This also fits the systems behavior: as battery voltage drops, at some point the +-15V DC/DC converters fail which power the OPAMP measuring circuits. This results in false measurement data but it is still sent down to ground

station by the communications link. As the voltage drops lower, it ultimately dips below the logic level voltage of the Arduino and communication is lost. All in all we attained almost double the flight time which we designed for.

5. RESULTS

All data show consistent I-V measurements, yielding a data set of 192000 I-V characteristics acquired at a steady interval throughout the whole flight.

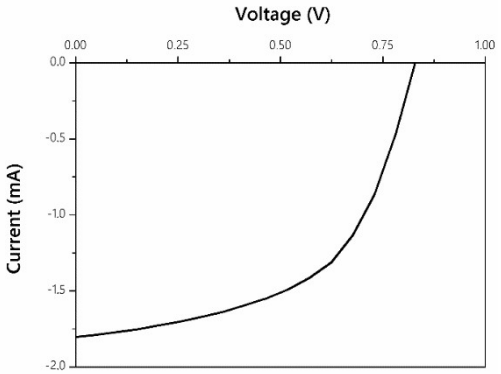

Figure 7 – Example I-V curve acquired in the stratosphere through the BCF circuit.

The main focus of this communication however lies with the measuring system itself. The performance thereof is monitored by adding a reference resistor to one of the MUX channels of each measuring circuit. Assuming the value of this resistor remains unchanged during flight, every observed change in its I-V curve can then be traced back to an inconsistency in the monitoring system's performance. Since the I-V curve of a resistor is a straight line with the slope indicating value of resistance, observing the evolution of this measured slope over time in this case indicates system behavior. Slopes were derived from the 20 point I-V curves by performing linear regression and taking the regression coefficient. To make up for the different resistor values used on BCF vs DEdiode sample group measuring circuits, the relative change ($\Delta val/val_0$) of regression coefficient is plotted as a function of sweep number. Sample group A's measuring circuit was not equipped with a reference resistor. Its performance is therefore not monitored separately.

Fig. 8 depicts this evolution of reference resistor measurements throughout time for the BCF1, BCF2, DEdiode1, DEdiode2 and DEdiode3 measuring circuits. The measured resistance is clearly not the constant value which would be expected for a steady measuring setup performance when assuming unchanged resistance value. On plain sight, all 5 graphs exhibit the same trend of rises and falls. Furthermore, deeper analysis proves a fixed gain difference between the graphs of BCF circuits when compared to DEdiode.

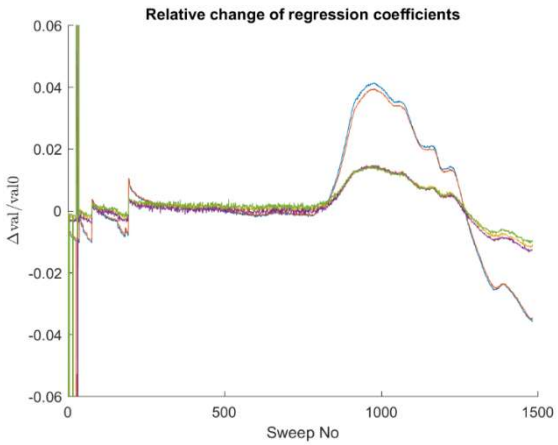

Figure 8 – Relative change of regression coefficients as a function of sweep number. BCF1 in red, BCF2 in blue, DEdiode1 in yellow, DEdiode2 in green and DEdiode3 in red.

6. CONCLUSIONS

The OSCAR project successfully designed, built and launched a solar cell performance monitoring system for space-like environments. The system performed steadily throughout its 4h flight time and reported an extensive amount of data on novel thin film solar cells exposed to the conditions of a stratospheric balloon flight. The measuring setup itself indicates similar drifts on each of the subcircuits. Moreover, this drift varies between sample group measuring circuits with a fixed gain, indicating a shared external influencing parameter with different levels of significance between BCF and DEdiode. This could be justified from the usage of different reference resistors with different thermal coefficients for each. The influencing parameter would in this case be ambient temperature and not have its biggest influence on the measuring setup itself, but on the resistors used to monitor its behavior. A follow-up experiment to assess this prediction would consist of comparing 2 cases where we again perform the same measuring system performance monitoring in a climate chamber. The measurement board would, for each BCF and DEdiode measuring subcircuit, be externally connected to a resistor identical to its internal reference resistor via the edge connector. In the first case both the measuring board with internal reference resistors as well as the externally connected resistors would be thermally cycled. In the second case only the externally connected resistors would be thermally cycled while the measurement board and reference resistors are kept stable. A comparison between both should clearly indicate the influence of temperature on the measurement board and its subcircuits on their own.

7. REFERENCES

[1] R. L. Easton and M. J. Votaw, “Vanguard I IGY satellite (1958 beta),” *Rev. Sci. Instrum.*, vol. 30, no. 2, pp. 70–75, 1959.

[2] F. A. Lindholm, J. G. Fossum, and E. L. Burgess, “Application of the Superposition Principle to Solar-Cell Analysis,” *IEEE Trans. Electron Devices*, vol. 26, no. 3, pp. 165–171, 1979.